Technical Report NAS-MSFC-1

STEREOSCOPIC ANALYSIS OF POLLUTED AIR MASSES

by

W. Z. Sadeh*

Fluid Dynamics and Diffusion Laboratory
Department of Civil Engineering
Colorado State University
Fort Collins, Colorado

Prepared for
Aerospace Environment Division
George C. Marshall Space Flight Center
National Aeronautics and Space Administration
Contract No. NAS8-25236

May 1973

CER72-73WZS31

*Associate Professor of Engineering

ABSTRACT

Air pollution levels depend strongly upon the spatial and time variations of various pollutant concentrations. In the vicinity of pollution sources locally high concentrations and significant variation with time of pollutants occur. Surveillance of pollutant concentrations and dispersion requires adequate monitoring over large relevant areas at fixed time intervals. Particularly, strong and stable temperature inversion can cause such circulation conditions where vertical mixing of pollutants is prohibited.

Remote sensing by means of stereo images obtained from flown cameras and scanners provides the potential to monitor the dynamics of pollutant mixing over large areas. Moreover, stereo technology permits efficient monitoring of pollutant concentration and mixing with sufficient detail. Consequently, regional standards on air quality can be set forth. Furthermore, methods to detect unpredicted and significant pollution variations can be developed. A method of remote sensing using stereo images is described. Preliminary results based on comparison with ground measurements by alternate method, e.g., remote hot-wire anemometer technique, are supporting the feasibility of stereo analysis using aerial cameras.

INTRODUCTION

Broadly, changes in the constituents of air either by addition to and/or subtraction from them which affect the physical and/or chemical properties of the air, and subsequently cause detectable deterioration of air quality may be defined as air pollution. Pollutants include any natural and artificial, i.e., man-made, contaminants capable of altering air properties and being airborne. Air pollutants occur in the form of gases, liquid droplets and solid particles, both separately and in mixtures. Gaseous pollutants constitute approximately 90% of the total mass entering the atmosphere. The other 10% are made up of particulates and liquid aerosols [1]. Pollutants emitted directly from identifiable sources are classified as primary pollutants. On the other hand, pollutants produced by interactions among primary pollutants or by reactions with atmospheric constituents are categorized as secondary pollutants [2]. These pollutants are hazardous and particularly health endangering. By and large, the most harmful air pollution is due to the production of acid droplets through the interaction of sulfuric and nitric oxides with humid air. These oxides evolve primarily from combustion of fossil fuel and refuse.

A complete description of polluted air masses is quite difficult since generally the polluting entities do not retain their exact identities after entering the atmosphere. The pollutants undergo thermal and photochemical reactions, and continuous spatial and time variations. In the vicinity of polluting sources locally high concentrations and significant changes with time occur. Subsequent dispersion depends strongly upon the prevailing winds, atmospheric stability and topographic features. Levels of pollutants are determined in terms

of areal concentration density, i.e., concentration per unit area. Similar health hazards can arise from short time exposure of order of few minutes to locally high concentrations, or in the case of long time exposure of hours and even days but to low concentrations.

Detection of pollution through direct sampling is rather complex since a great number of sampling stations distributed over large areas are needed. In United States there are over 7,000 sampling stations [1]. Most of these stations are located in the vicinity of major point sources such as high smoke stacks, and in metropolitan and industrial areas, i.e., in area sources. To monitor the spacial and time variations of pollutants in order to obtain contour maps of trace constituents, surveys within relatively large distances downstream of the sources are required. For instance, aerial photographs of power plants reveal that the most dangerous surface pollution concentrations occur within 4 to 8 km downwind of the plants [3]. Surveys of plume rise and dispersion over such large areas using sampling stations are costly and inherently difficult due to the continuous changing meteorological conditions. Moreover, the use of sampling stations to monitor line sources such as highways and runways, mobile sources, and unpredictable downwind precipitation areas is practically precluded due to the extreme range of area involved and concentration changes. In many cases, furthermore, the setup of sampling stations is prevented by local safety regulations, e.g., erection of tall meteorological towers in vicinity of airports.

Pollutants are deposited into the atmospheric boundary layer where they are conveyed either as active or passive scalars by advection and turbulent diffusion. In the atmosphere the turbulent diffusion depends on both shear flow and vertical temperature distribution. The buoyancy

forces, which are determined by the temperature variation, play a prime role in the dynamics of air motion. When stable conditions prevail, i.e., subadiabatic temperature lapse rates, the turbulent diffusion of contaminants is retarded by buoyancy forces. The extreme case of stable conditions is represented by temperature inversions. Strong and stable inversion layers yield extreme circulation conditions where vertical turbulent mixing of pollutants is effectively prohibited by the temperature lid. Dangerous inversion which can persist for several days usually develop within high pressure ranges. Over urban areas temperature inversions are commonly found beyond a certain mixing depth [4,5]. Generally, the urban inversions arise in the form of a dome-shaped envelope due to the uneven heat distribution. Furthermore, on clear mornings at sunrise and often on evenings at twilight with light winds or calm conditions near the surface, a base inversion layer occurs. This layer may extend from the ground up to heights of 150 to 750 m depending upon the local topographic configuration [6]. Simultaneously, a second inversion layer may exist at higher altitudes [6]. Inside the inversion layer the contaminants are uniformly distributed. Usually, highest surface concentrations occur within 5 to 10 km downwind of the sources and can persist for several days.

Air pollution surveys are strongly dependent on detailed knowledge of prevailing turbulent winds and atmospheric stability conditions within relevant large areas. Remote-sensing technology possesses the potential to monitor both meteorological parameters and needed data on the dynamics of mixing of pollutants in sufficient detail and within substantial large areas. The orbital stereo photographs taken during the Gemini missions clearly substantiate the use of stereo techniques

to survey contaminated air masses over exceedingly large areas [7]. Furthermore, advance detection of unexpected pollution is feasible. As a result, adequate regional air quality standards and control regulations can be set forth. However, to determine chemical composition of pollutants, size and distribution of particulates, health endangerment levels and so on, direct sampling is needed. Remote sensing by means of stereoscopic observations is capable of yielding a host of information which can augment manifold the knowledge on the dynamics of mixing of pollutants and surface concentrations.

ANALYSIS OF STEREOSCOPIC IMAGES

Stereoscopic viewing of targets essentially reduces to stereo comparison of a pair of images with some overlapping areas. Such two successive photographs can be taken by a precision aerial camera along the flight path of an aircraft. Two pictures taken in succession and the corresponding overlapping areas indicated by shaded regions I and II are shown in Fig. 1(a). Next, two arbitrary objects are selected within the area of overlap. They are denoted by 1 and 2 in the first photograph while their conjugate images in the second picture are designated by 1' and 2', respectively. These objects can be a sharp ground feature and a tenuous but visible polluted air mass as portrayed in Fig. 1(b). Under the assumption of unmovable pollution target, the height and three-dimensional extent of the plume can be determined by stereoscopic comparison of the two images [8]. Thus, the time lapse between two successive exposures must be short enough such that the distance traveled by the pollution target can be disregarded. The human matching of the stereo images is carried out using a stereocomparator. Subsequent attempts to

align the pollution target will lead to a mismatch for the ground object. This misalignment is caused by the fact that the two targets are situated at different heights. The distance difference, i.e., the parallactic distance, can be estimated from the mismatch of the ground reference object as illustrated in Fig. 1(b). Then, the height of the pollution target is strated in Fig. 1(b). Then, the height of the pollution target is computed by triangulation utilizing the parallactic distance and the difference in the view angles from the two images for the pollution target (the parallactic angles). This method can also be used to estimate the features of an inversion layer. When the motion of the polluted mass is not negligible, a third stereo image is needed. Then, two independent parallactic distances are obtained. Similar triangulations yield both plume altitude and its horizontal velocity.

Results using this stereo analysis to deduce the three-dimensional extent of visible plumes are reported in Ref. 9. The three-dimensional extent of plumes were estimated using vertical and oblique stereo image pairs with 60% overlap taken at altitudes of 10,000 and 15,000 ft, respectively. The accuracy of this method decreases drastically with distance from the source. At 3 miles downwind of the polluting source, the error in approximating the plume height is ±100 ft [9]. Beyond this range, evaluation of plume height becomes uncertain. Human photogrammetric stereo comparison is limited even under optimum conditions. For barely visible and invisible plumes such as oxide gases, human stereo interpretation is completely impractical. With increased use of precipitators in high smoke stacks, the visibility problem becomes more compound.

The stereoscopic analysis of images is highly improved and refined when adequate digital cross-correlation techniques are utilized. Initially, these techniques were developed and successfully employed for remote measurement of sound sources, heat radiation, wind, and turbulence using passive optical crossed beams [10,11,12]. The crossed-beam correlation method was further applied to active sensors. An extensive review of the applications of electromagnetic correlation techniques can be found in Ref. 13. Basically, this method combines remote measurements with adequate data processing and statistical analyses.

To carry out digital correlation of a stereoscopic image pair, conversion of each picture into discrete scan lines is necessary [14]. These lines, which are depicted in Fig. 1(a), can be obtained by scanning stereo photographs with a microdensitometer [9,15]. Essentially, the discrete scan lines constitute the scan history of the image in the form of a digitized record of the radiation power within a certain field of view. Thus, the scan history consists of a sufficient number of adjacent scan lines which supply an image of the target area in terms of a strip map. It is, further, important to note that scan histories within wavelength ranges where photographic emulsions are not available can be supplied by utilizing electromechanical stereoscopic scanners.

The scan history can be expressed in terms of a signal

$$x(t) = x(m,n) \quad , \tag{1}$$

where m designates the scan line number relative to the position of a ground reference object whose scan line is $m = 0$. The sample point number along a particular scan line is denoted by n. It is determined

with respect to the sample point $n = 0$ that intersects the ground reference feature.

The stereo analysis is performed by computing the cross-covariance function of the two overlapping areas I and II. To calculate the cross-covariance, one of the images, e.g., image II, is delayed by k scan lines and ℓ sample points. Then, the sample cross-covariance estimate is

$$C_{xy}(k,\ell) = \frac{1}{4MN} \sum_{-M}^{M} \sum_{-N}^{N} x(m,n)y(m+k,n+\ell) \quad , \tag{2}$$

where $x(m,n)$ is the signal from image I, and $y(m+k,n+\ell)$ is the delayed signal from the overlaying area II. The number of resolution elements per strip is denoted by $4MN$. A direct quantitative measure for the matching is provided by the cross-covariance. The best match of the features related to the polluted mass is indicated by the peak value of the cross-correlation. Similarly, the best match for the ground reference object is also furnished by the cross-covariance. As a result, the parallactic distance is obtained and, then, the plume features (or inversion characteristics) are evaluated by triangulation as portrayed in Fig. 1(b).

The signals from stereo images are random variables of time and, thus, they can be expressed as

$$x(t) = x_1(t) + x_2(t) \quad , \tag{3.1}$$

and

$$y(t) = y_1(t) + y_2(t) \quad , \tag{3.2}$$

where the subscripts 1 and 2 denote the target signal and transmission noise, respectively. Then, the cross-covariance is

$$\overline{C_{xy}(\tau)} = \overline{x_1(t)\, y_1(t+\tau)} + \overline{x_1(t)\, y_2(t+\tau)} + \overline{x_2(t)\, y_1(t+\tau)} + \overline{x_2(t)\, y_2(t+\tau)} \quad , \tag{4}$$

where the τ designates the delay time, and the overbar denotes time integration over the entire scan history. The first term on the right-hand side of Eq. (4) is the cross-covariance of the common signals. This product is always positive since both signals are of the same sign being generated by the same random process. In other words, both stereo images are affected in a similar way by the polluted air mass target. This is true provided that the pollution target is unmobile. The other three products represent cross-covariances of uncorrelated random variables caused by statistically independent random processes. Consequently, they vanish provided that the integration time is long enough. It is, further, important to note that the cross-covariance is dominated by the produce $\overline{x_1 y_1}$. This term increases linearly with integration time. On the other hand, the other produces oscillate with equal likelihood about the average value. Furthermore, their contributions to the time integral increase with the square root of integration time [12]. Adequate averaging methods to cancel the noise by product integration for finite integration time are proposed in Ref. 12.

The mean square error of the cross-covariance estimate due to individual resolution element (or finite integration time) is given by the variance,

$$\mathrm{Var}[C_{xy}(k,\ell)] = \frac{1}{4MN-1} \sum_{m,n} [x(m,n)y(m+k,n+\ell) - \overline{C}_{xy}]^2 \quad , \tag{5}$$

since $C_{xy}(k,\ell)$ is an unbiased estimate of the true value of the cross-covariance $\overline{C}_{xy}$ [16]. This error decreases with increasing

integration time. Next, the confidence to obtain a meaningful match is expressed by the ratio of the cross-covariance estimate to its root-mean-square (rms) error

$$\alpha_{k,\ell} = \frac{C_{xy}(k,\ell)}{\sqrt{\text{Var}\ [C_{xy}(k,\ell)]}} \quad , \tag{6}$$

which is the coefficient of confidence.

In practice, additional limitations exist due to uncontrolled variations of the optical environment. Averaging techniques which can efficiently eliminate, to a large extent, these effects were developed [12]. These techniques employ the variations of piecewise mean values to recognize and eliminate this noise. A sample of the instantaneous product xy of two total signals for two different wavelength ranges from a stereo scanner is shown in Fig. 2. The continuous strongly oscillating curve represents the scan time history. The cumulative average of the instantaneous product

$$C_{xy}(k,\ell,\ T) = \frac{1}{T} \int_0^T x(t)y(t)dt \quad , \tag{7}$$

is a function of the variable record length (or integration time) since $0 < T < 2MN$. With increasing record length (or integration time) the variations of the cumulative average diminish since the changes in the instantaneous product cancel each other. As mentioned earlier, the contribution of the common signals from the polluted mass to the instantaneous product is positive. Thus, the negative fluctuations of the instantaneous product represent signal components which are unrelated to the target. Moreover, the positive instantaneous products also contain signals which are uncorrelated to the pollution target. These

positive products cancel the negative products. The shaded areas in Fig. 2 delineates the power of the unrelevant signals. Their cancellation through the integration process is indicated by the decreasing change in the variations of the cumulative average. Furthermore, with increasing number of instantaneous products the mutual cancellation of the unrelated signals is enhanced. This process of cancellation by product integration is completed when the cumulative average reaches a constant value [12,14]. Practically, this value represents the power of the common signals from the pollution target. Consequently, the product integration process permits recovery of very weak signals provided that the target is sufficiently large and homogeneous. The latter condition is needed to allow complete supression of the noise [12]. This method can be further utilized for nonhomogeneous polluted masses by subdividing it into homogeneous domains. This can be achieved using recently developed unsupervised classification methods [14]. As a result, even invisible pollution targets are eventually retrievable using this stereo correlation analysis. Furthermore, this technique can be applied to evaluate the water vapor burden within a column of air.

EXPERIMENTAL RESULTS

To demonstrate the feasibility of stereoscopic remote sensing of polluted air masses and of stereo-correlation analysis of stereoscopic images, an extensive field experimental program is currently being conducted. The objectives of the field experiment could not be achieved by simply surveying pollutants randomly emitted into the atmosphere. Particularly, it was imperative to surmount the unpredictable effects of continuous changing meteorological conditions. It was further desired

to inject pollutants under controlled circumstances into a known environment.

For these reasons, it was decided to simulate the environmental conditions using the wake flow produced by a 10 ft diameter fan of variable pitch (Hartzell A120-6). This fan constitutes the core of the Colorado State University Environmental Field Station. The fan is driven by an internal combustion engine and, hence, continuously variable air speeds up to 20 mph can be generated. Within the wake large scale turbulence is produced and, consequently, the environmental conditions are adequately simulated for pollutant injection. To reduce undesirable interferences with the ambient winds, all experiments were conducted under calm conditions or light winds up to at most 2 mph. Continuous monitoring of the prevailing winds was performed using cup anemometers.

Contaminants in the form of gases, liquid aerosols and particulates can be released under governed conditions from point sources and/or line sources. The pollutants may be emitted either separately or premixed in any desired ratios. Locations of polluting sources were selected based on velocity distribution and turbulence characteristics within the wake. Moreover, since the sources are mobile they can be located in any configuration and at any position of interest. It is worth pointing out that same sources can be utilized to generate controlled water vapor plumes within the wake.

The Environmental Field Station is located on a flat surface free of immediate natural or artificial obstructions. Almost daily base temperature inversions on clear mornings and on evenings at twilight occur at its site. The station is equipped with an analog Data Acquisition

System. In addition, a digital Data Acquisition System is available for on-line data reduction and analysis. Fixed ground reference targets needed for the stereo photographs were set up.

To ascertain the practical applications of the stereoscopic remote sensing, simultaneously with the aerial stereo survey ground measurements are necessary. Furthermore, comparison of the results will lead to development of adequate calibration techniques for the stereo remote sensing. Ground measurements of velocity and turbulence were carried out utilizing a novel three-lead hot-wire anemometer system conceived, designed and built at Colorado State University [17]. This new system permits remote use of hot-wire anemometers since the cables connecting the hot wire, i.e., the sensor, to the bridge can exceed 500 ft in length. In the past, the length of the connecting leads was limited to about 25 ft [17]. The new remote system affords innumerable applications of hot-wire anemometry techniques in atmospheric measurements. Specific hot-wire interpretation methods developed for flow with large fluctuations, such as encountered in the atmosphere, are employed [18].

The aerial stereoscopic photographs were taken employing a Wild RC8 automatic precision mapping camera system with 93° coverage (Wild-Heerbrugg Inst.). The camera is equipped with a 6 in Universal Aviogon lens cone (f/5.6) with rotary shutter. An antivignetting filter Wild A.V. 2.2 x (Wild-Heerbrugg Inst.) is utilized to provide uniform lighting across the lens and, thus, uniform exposure on the film is obtained. All pictures were taken using Kodak aerocolor negative estar base film. Included in the camera system are a driving mechanism, a control box, a viewfinder telescope, a clock and an altimeter. A general view of the camera system is shown in Fig. 3. The camera produces 9 x 9 in photographs

with remarkably low distortion and high resolution. The former is smaller than 0.01 mm whereas the latter varies from 50 lines/mm in the center to 25 lines/mm in the corners. This high resolution permits adequate conversion of the picture into discrete scan lines. Since the film advance per exposure amounts to 10 in, the readings of the incorporated clock and altimeter can be recorded on each photograph. Continuous adjustment of the exposure time from 1/100 to 1/700 sec is provided by the driving motor. Four overlap areas of 20, 60, 70 and 80%, respectively, are available. The shortest time interval between exposures, i.e., the time lapse, is roughly 3 to 3.5 sec. A plume conveyed by such a velocity that the distance traveled during the time lapse is small compared with its overall horizontal extent, it will appear on two successive photographs as being approximately stationary. At this point, it is important to notice that the plume is "stationary" with respect to stereoscopic photography since it will roughly affect a stereo-image pair in the same manner as a ground reference object. Thus, one can consider the plume of being stereoscopically stationary. Such situations occur particularly within inversion layers, light winds or calm conditions. For aerial operation, the camera system is flown in Colorado State University Aero-Commander 500B research aircraft.

Direct measurement and recording of the space coordinates of any desired image on the stereo-photograph pair is carried out utilizing the Wild STK-1 Stereocomparator/Digitizer/IBM Card Punch (Wild-Heerbrugg Inst.). The coordinates of selected objects can be measured with a precision of 1μm (1/25,400 in). Algorithms for determination of the space coordinates were put forth. It is important to remark that the evaluation of the vertical coordinates may be arduous due to the

haze of the plume. Scanning by means of a microdensitometer, which measures the transmittance of the photographic emulsion, can undoubtly supply more reliable estimation of the vertical extent of the pollution target.

Henceforth, the preliminary results of the feasability investigation are presented. To begin with, intensive, albeit not exhaustive, visualization studies of circulation of visible plumes generated by colored smoke were conducted. The smoke point sources were located at various positions along the streamwise direction of the wake flow and at several elevations above the ground. Several frames from a movie showing the smoke plume circulation, entrainment and dispersion without and with temperature inversion are given by Fig. 4. The fan is also shown in Fig. 4(a). Powerful and relatively large scale vortices were clearly discerned when unstable conditions (superadiabatic lapse rates) prevailed. The photographs shown in Figs. 4(a) and 4 (b) were taken under such conditions. Without temperature inversion, the vortices disperse quickly the smoke plume at higher altitudes. However, in the neighborhood of the sources, due to the large scale vortices, deposit of pollutants on the ground can occur as indicated by the smoke circulation observed in Fig. 4(b). On the other hand, under inversion conditions small scale vortices were prominent as illustrated by the photographs shown in Fig. 4(c). Relatively high smoke concentrations persisted for prolonged time. Knowledge of the scale of vortices is essentially for study of both dispersion and concentration of pollutants, and temperature distribution. Particularly, within the earth-atmosphere interface, the prevailing vortices play a prime role in the surface concentration of pollutants.

Next, numerous overflight surveys of the smoke plume were carried out. Stereoscopic photographs were taken from several altitudes. All photographs were obtained with 60% overlap and with a time lapse of 3 sec. The aerial photogrammetric surveys were conducted either under calm conditions or light winds up to about 1 mph, and temperature inversion. A stereo-image triplet of smoke circulation taken from an altitude of 2000 ft is shown in Fig. 5. Analysis of the stereoscopic photographs by means of a stereocomparator revealed that the maximum windwise extent of the plume was about 70 ft. The shape and extent of the smoke plume in the horizontal plane is depicted in Fig. 6. For a wind speed of 1.5 ft/sec (~ 1 mph), the smoke plume traveled a distance of 4.5 ft during the time lapse. Since this distance is about 6.4% of its windwise range, one can conceivably assume that, for any practical purposes, the plume is stereoscopically stationary. The similar extent of the smoke plume obtained by comparison of a series of stereo images taken under same conditions substantiates the foregoing conclusion.

Basically, the smoke plume was produced by injecting smoke into the wake. Subsequently, the smoke was transported by the wake flow. Hence, the wake can be considered of being an invisible plume whose overall spatial extent should coincide with this of the visible smoke plume. To corroborate the results obtained by the remote stereo analysis, hot-wire anemometer ground measurements of the planar extent of a corresponding invisible plume were performed. These measurements were conducted under same wind and inversion conditions as for the remote stereoscopic survey but not simultaneously. The boundary of the invisible plume, i.e., the wake boundary, was defined as the location

where the local axial velocity reduces to about 2% of the fan rotor tip velocity [19]. The results of the hot-wire anemometer survey are shown in Fig. 6 together with the horizontal extent of the visual smoke plume. A striking similarity between the extent of the visible plume, deduced by means of remote stereo analysis, and the invisible plume, obtained through ground measurements, is clearly discerned. This consistent general congruence substantiates the feasibility of stereoscopic remote sensing. Furthermore, this remarkable agreement was obtained for a relatively small, tenuous plume. Thus, the stereo remote sensing can be used to survey even barely visible and weak plumes. Currently, the evaluation of the three-dimensional features of the plume is underway.

CONCLUDING REMARKS

The feasibility of stereoscopic remote sensing of polluted air masses by means of flown stereo cameras is indicated by the preliminary results presented in this work. The evaluation of the planar extent of a plume based on both stereo analysis and ground measurements exhibits a striking congruence. Even barely visible and tenuous plumes of relatively limited spacial extent can be monitored by stereo techniques. In this experiment, the windwise extent of the plume was roughly 70 ft.

Stereoscopic analysis of a stereo-image pair can be used to establish the features of a polluted air mass provided that the condition of stereoscopic stationarity is satisfied. Basically, when the distance traveled by a plume during the time lapse between two successive exposures is small compared with its overall horizontal extent, one can assume that the plume is stereoscopically stationary. This situation usually occurs within temperature inversion layer, under light winds or calm

conditions. When the condition of stereoscopic stationarity is not fulfilled, e.g., strong winds, a stereo-image triplet is necessary. Currently, stereo comparison analysis of such triplets is being carried out.

By and large, standard stereo comparison analysis is limited due to variations in the concentration of pollutants within the plumes, the haze of the plumes, and the continuous changing optical backgrounds. Digital stereoscopic analysis based on correlation techniques possesses the potential to overcome these difficulties. An intensive effort to demonstrate the efficacy of digital stereo correlation is planned. The development of mathematical models for long term pollution distribution and concentration over large areas depends, to a large extent, on detailed knowledge of both meteorological conditions and polluted air masses features. Stereoscopic techniques can be used efficiently to provide contour maps of pollution including isoconcentration density curves in addition to meteorological parameters.

Basically, stereoscopic remote sensing of polluted air masses by flown stereo cameras permits adequate monitoring within large areas at selected time intervals. Furthermore, unpredicted and unexpected pollution can be detected. Consequently, air quality standards and control regulations can be set forth.

REFERENCES

1. Morgan, G. B., Ozolins, G. and Tabor, E. C., "Air pollution Surveillance Systems," Science, 170, 3955, 289-296 (1970).

2. Chambers, L. A., "Classification and Extent of Air Pollution Problems," Air Pollution, edit., Stern, A. C., Vol. 1, Air Pollution and Its Effects, 1-22, Academic Press, New York 2nd ed. (1968).

3. Krause, F. R., Private Communication, NASA, Marshall Space Flight Center, Huntsville, Alabama (1972).

4. Hoffert, M. I., "Atmospheric Transport, Dispersion, and Chemical Reactions in Air Pollution: A Review," AIAA Journal 10, 4, 377-387 (1972).

5. Davidson, B., "A Summary of the New York Urban Air Pollution Dynamic Research Program," J. Air Pollution Control. Assoc., 17, 3, 154-158 (1967).

6. Wanta, R. C., "Meteorology and Air Pollution," ibid. Ref. 2, 187-226.

7. Wobber, F. J., "Orbital Photos Applies to the Environment," J. Photogrammetric Eng., 26, 8, 852-864 (1970).

8. Moffitt, F. H., Photogrammetry, International Textbook Co., Scranton, Penn., 2nd ed. (1967).

9. Veress, S. A., "Air Pollution Research," J. Photogrammetric Eng. 26, 8, 840-848 (1970).

10. Fisher, M. J. and Krause, F. R., "The Crossed-Beam Correlation Technique," J. Fluid Mech., 28, 4, 705-717 (1967).

11. Krause, F. R., Derr, V. E., Abshire, N. L., and Strauch, R. G., "Remote Probing of Wind and Turbulence Through Cross-Correlation of Passive Signals," Proceedings, 6th International Symposium on Remote Sensing of Environment, 13-16 October 1969, Univ. of Michigan, Ann Arbor, Mich., 327-257 (1969).

12. Krause, F. R., Su, M. Y. and Klugman, E. H., "Passive Optical Detection of Meteorological Parameters in Launch Vehicle Environments," J. Applied Optics, 9, 5, 1044-1055 (1970).

13. Krause, F. R., edit., "Research on Electromagnetic Correlation Techniques," NASA TM X-64505, Marshall Space Flight Center Huntsville, Alabama (1970).

14. Krause, F. R., Betz, H. T. and Lysobey, D. H., "Pollution Detection by Digital Correlation of Multispectral Stereo-Image Pairs," AIAA Paper No. 71-1106, Joint Conference on Sensing of Environmental Pollutants, 8-10 November 1971, Palo Alto, Calif. (1971).

15. Data Corporation Manual, "Man-Data Micro-Analyzer," Data Corp. Dayton, Ohio (1968).

16. Bendat, J. S. and Piersol, A. G., Random Data: Analysis and Measurement Procedures, Wiley-Interscience, New York (1971).

17. Sadeh, W. Z. and Finn, C. L., "A Method for Remote Use of Hot Wire Anemometer," Review Scient. Instrums., 42, 9, 1376-1377 (1971).

18. Sadeh, W. Z., Maeder, P. F. and Sutera, S. P., "A Hot Wire Method for Low Velocity with Large Fluctuations," Review Scient. Instrums., 41, 9, 1295-1298 (1970).

19. Koper, C. A., Jr., and Sadeh, W. Z., "A Preliminary Study of a Fan Wake," RM CEM70-71CAK-WZS23, Dept. of Civil Eng., Colorado State University, Fort Collins, Colorado (1971).

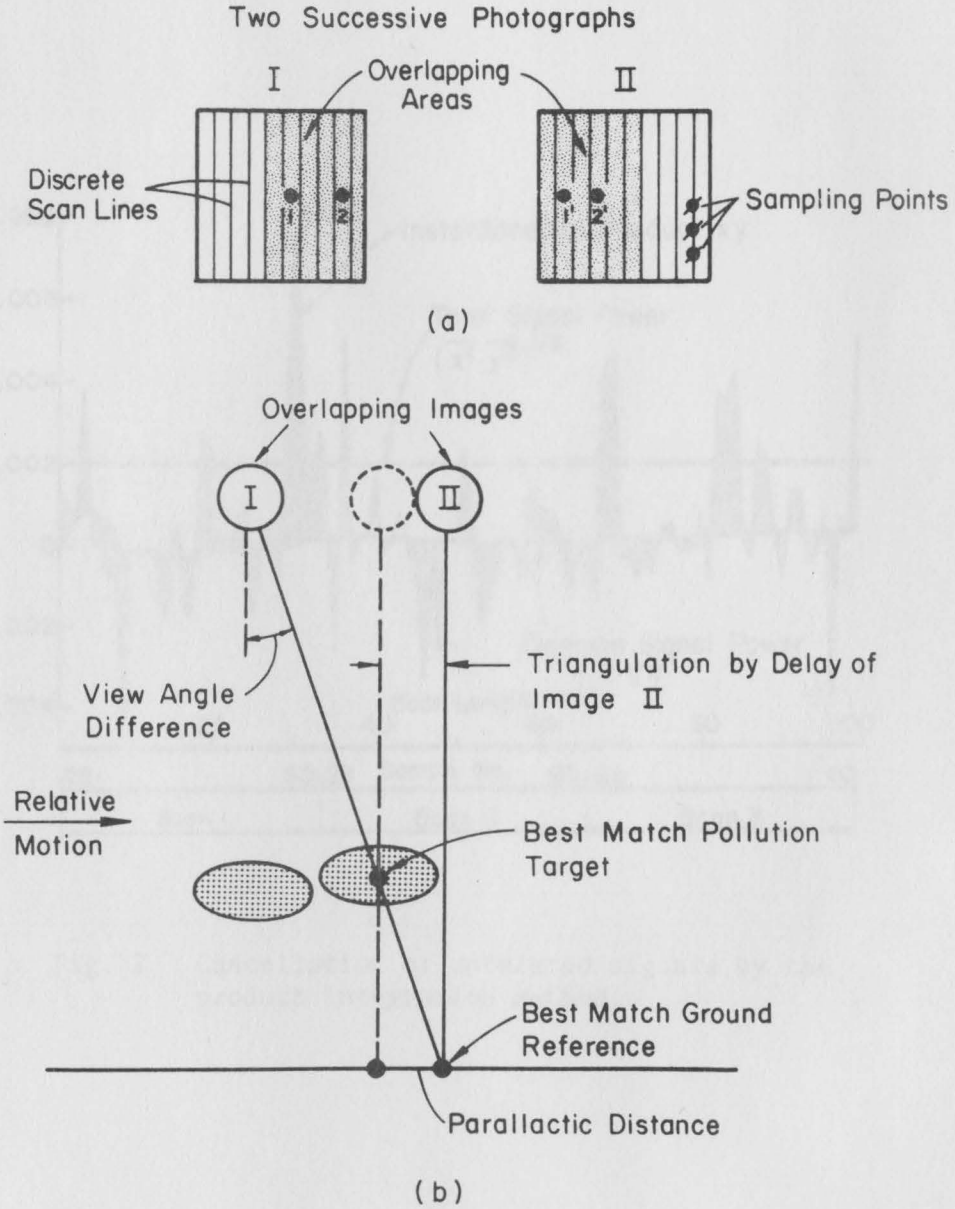

Fig. 1 (a) Stereoscopic imagery. (b) Determination of pollution target height by stereoscopic comparison and correlation techniques.

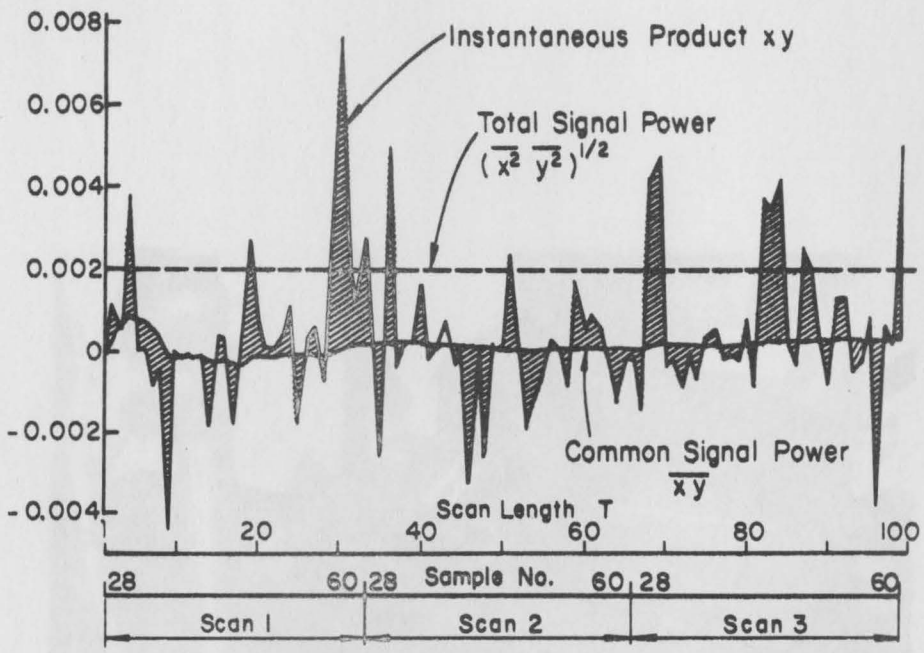

Fig. 2 Cancellation of unrelated signals by the product integration method.

Fig. 3 View of the Wild RC8 camera system.

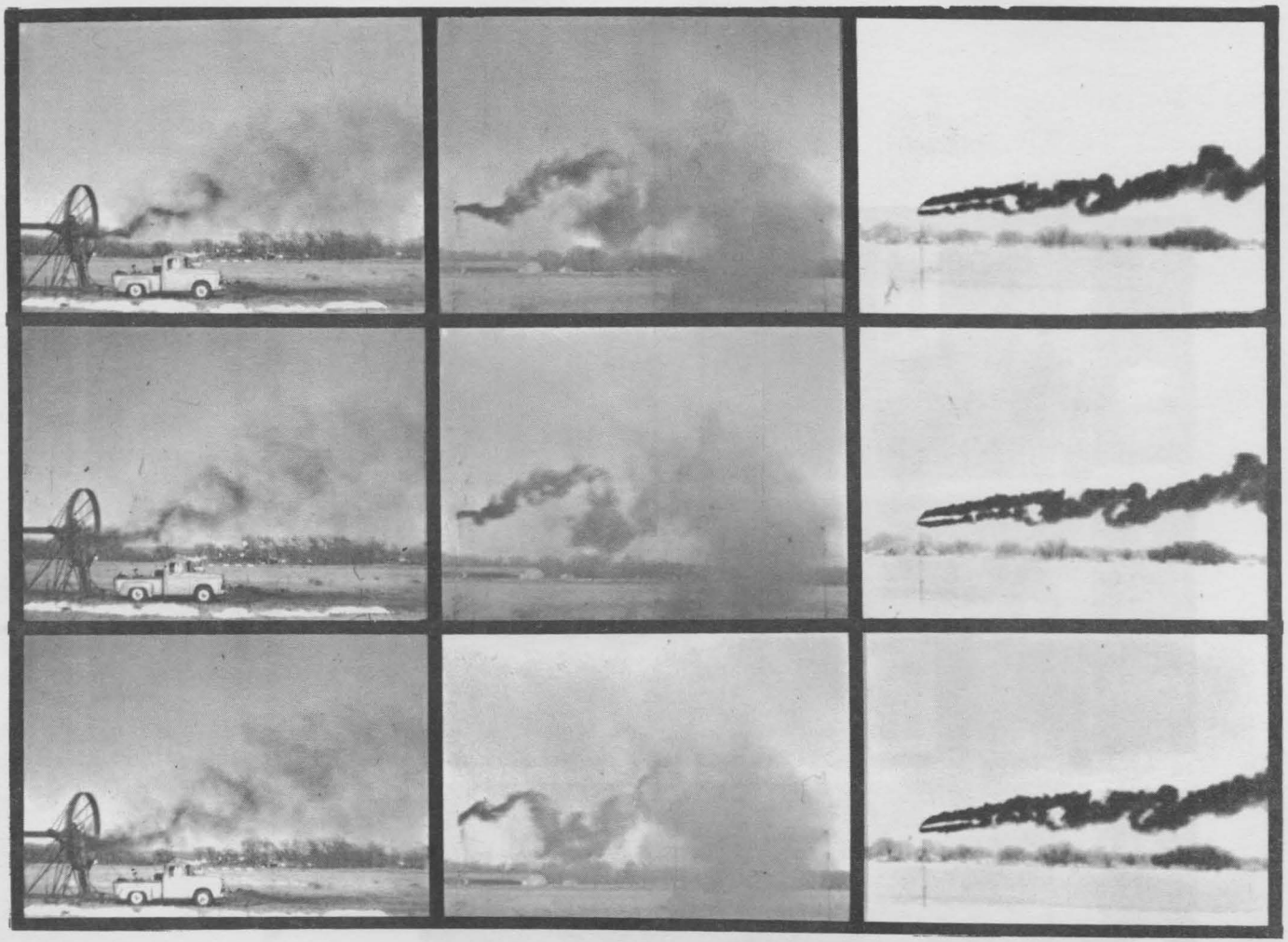

(a) (b) (c)

Fig. 4 Visualization of smoke plume circulation under unstable conditions: (a) point source upstream of the fan; and, (b) point source at 40 ft downstream of the fan; and within a temperature inversion layer: (c) point source at 150 ft downstream of the fan.

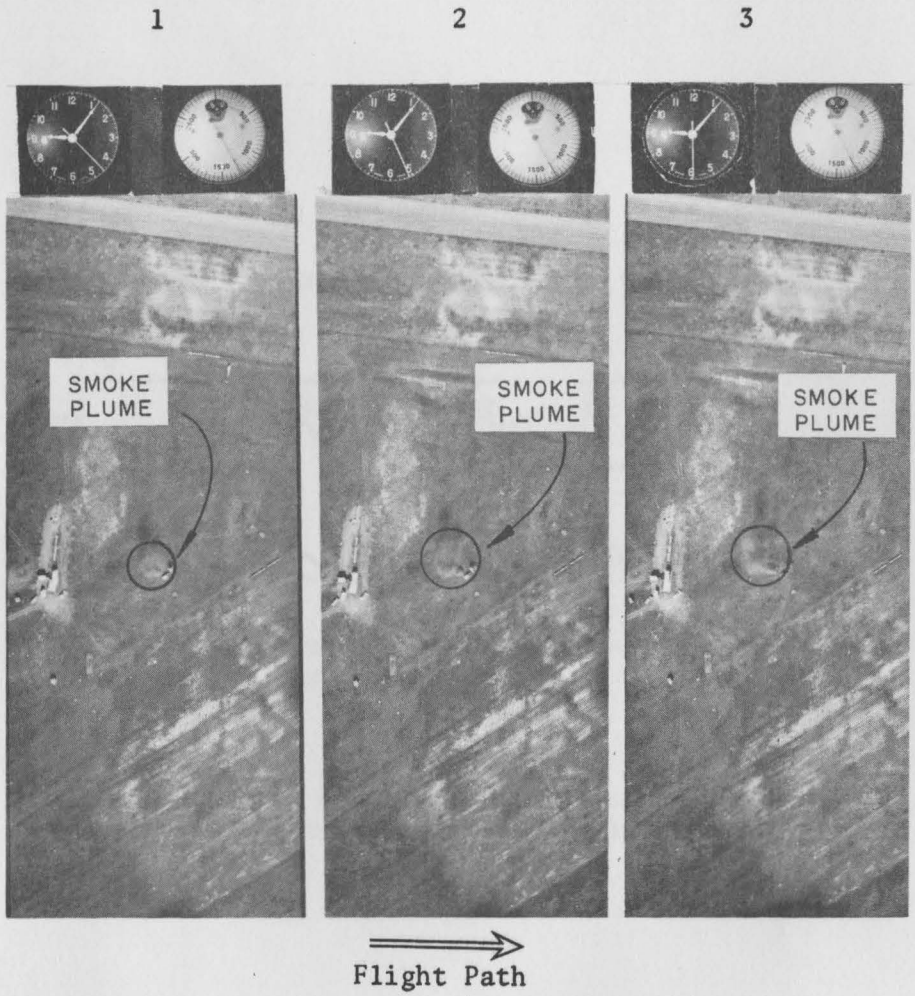

Fig. 5 Reproduction of colored stereo-image triplets of smoke circulation taken from an altitude of 2000 ft.

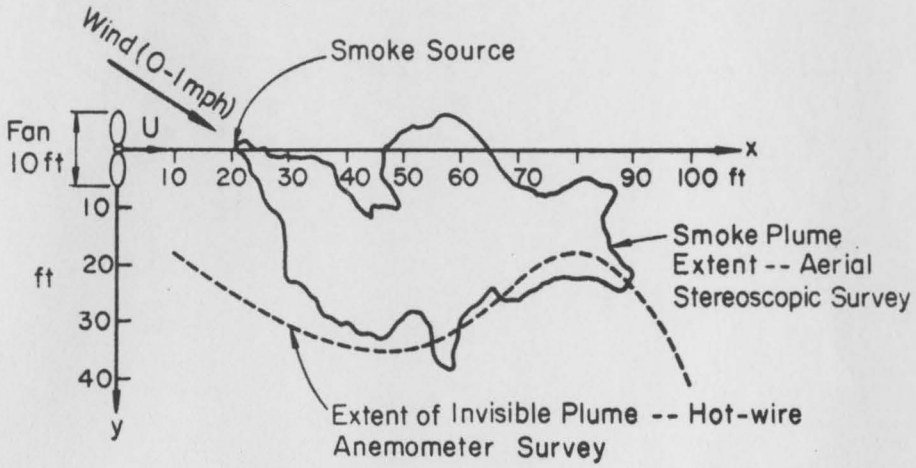

Fig. 6 Planar extent of visible smoke plume and its corresponding invisible plume.